

# Interpretation of the Scanning Tunneling and Atomic Force Microscopy Images of Layered Compound TlSbSe<sub>2</sub> by Electron Density Calculations

J. Ren and M.-H. Whangbo\*

Department of Chemistry, North Carolina State University,  
Raleigh, North Carolina 27695-8204

H. Bengel, H.-J. Cantow, and S. N. Magonov\*

Materials Research Center (F·M·F), Albert-Ludwigs University,  
D-7800 Freiburg, Germany

Received January 5, 1993. Revised Manuscript Received April 29, 1993

Atomic-scale scanning tunneling microscopy (STM) and atomic force microscopy (AFM) images were obtained for layered compound TlSbSe<sub>2</sub>. This compound consists of two slightly different TlSbSe<sub>2</sub> layers, and the surfaces of these layers have three different atoms. The observed STM and AFM images were analyzed by calculating the partial electron density  $\rho(r_0, e_f)$  and the total electron density  $\rho(r_0)$  of individual TlSbSe<sub>2</sub> layers. In both STM and AFM images, the brightest spots are associated with the most protruded surface atoms, i.e., the Tl atoms. For various bias voltages employed, there occurs no atom-selective imaging in the STM images.

## Introduction

Scanning tunneling microscopy (STM) and atomic force microscopy (AFM) are frequently applied for the examination of the surfaces of various materials.<sup>1,2</sup> These scanning techniques can provide atomic-resolution surface features. For many inorganic and organic crystals, the surface unit cell parameters of the STM and AFM images correspond well to those expected from the bulk crystal structures. However, the STM and AFM patterns within a unit cell can be strikingly different.<sup>3,4</sup> To a first approximation, the tunneling current from a surface is proportional to the partial electron density of the surface  $\rho(r_0, e_f)$ , at the tip-surface distance  $r_0$ , associated with the energy level  $e_f$ . (For metals,  $e_f$  refers to the Fermi level.<sup>5</sup>) In a contact mode of AFM operation, the repulsive interatomic forces between the scanning tip and the surface are probed.<sup>1,2</sup> Although the exact mechanism of atomic-resolution AFM imaging is not well understood, numerous studies have shown that this technique detects the periodic arrangement of atoms or molecules on various crystalline surfaces. The repulsive force the tip feels at a given location of the surface is expected to be proportional to the total electron density of the surface,  $\rho(r_0)$ . The STM and AFM images of several layered materials<sup>3,4,6</sup> and organic salt conductors<sup>7</sup> were successfully analyzed in

terms of their partial and total electron density plots, respectively.

The room-temperature ordered phase of TlSbSe<sub>2</sub> is a layered compound consisting of two slightly different layers (A and B) of composition TlSbSe<sub>2</sub> (Figure 1a).<sup>8</sup> The oxidation state of TlSbSe<sub>2</sub> may be described as Tl<sup>+</sup>Sb<sup>3+</sup>(Se<sup>2-</sup>)<sub>2</sub>. Each TlSbSe<sub>2</sub> layer has the structure of a double rock-salt layer, in which the Tl<sup>+</sup> and Sb<sup>3+</sup> ions are each surrounded by five Se<sup>2-</sup> ions in a distorted square pyramidal coordination. In each single rock-salt layer of TlSbSe<sub>2</sub>, rows of Tl<sup>+</sup> ions alternate with rows of Sb<sup>3+</sup> ions (Figure 1b). In the surface atom sheets of TlSbSe<sub>2</sub> layers A and B, the  $z$  coordinates of the Tl<sup>+</sup>, Sb<sup>3+</sup>, and Se<sup>2-</sup> ions are all different. (Here the  $z$  direction is perpendicular to the layer.) In both layers A and B, the Tl atoms are most protruded. In layer A, the heights of the Sb(1), Se(1), and Se(3) atoms are lower than that of the Tl(1) atom by 0.33, 0.43, and 0.26 Å, respectively (Figure 1c). In layer B, the heights of the Sb(2), Se(2), and Se(4) atoms are lower than that of the Tl(2) atom by 0.40, 0.47, and 0.44 Å, respectively (Figure 1d).

Since the Tl, Sb, and Se atoms have different sizes, the surface topography of layers A and B as seen by such surface probing techniques as STM and AFM may differ considerably from that expected on the basis of the crystal structure. In a recent STM study of TlSbSe<sub>2</sub>, Stocker et al.<sup>9</sup> suggested that the brightest spots of the STM image obtained at the bias voltage  $V_{\text{bias}} = -1.82$  eV result from the Tl<sup>+</sup> ions, but those obtained at  $V_{\text{bias}} = -1.65$  eV from the Se<sup>2-</sup> anions. Such an atom-selective imaging implies that the major orbital character of the occupied band levels

(1) Wiesendanger, R.; Güntherodt, H.-J., Eds. *Scanning Tunneling Microscopy*; Springer-Verlag: Heidelberg, 1992; Vols. I, II.

(2) Behm, J.; Garcia, N.; Rohrer, H., Eds. *Scanning Tunneling Microscopy and Related Techniques*; Kluwer Academic Publishers: Dordrecht, The Netherlands, 1990.

(3) Parkinson, B. A.; Ren, J.; Whangbo, M.-H., *J. Am. Chem. Soc.* 1991, 113, 7833.

(4) Magonov, S. N.; Zönchen, P.; Rotter, H.; Cantow, H.-J.; Thiele, G.; Ren, J.; Whangbo, M.-H. *J. Am. Chem. Soc.* 1993, 115, 2495.

(5) (a) Tersoff, J.; Hamman, J. R. *Phys. Rev. B* 1985, 31, 805. (b) Tersoff, J., in ref 2, p 77.

(6) Ren, J.; Whangbo M.-H. *Phys. Rev. B* 1992, 46, 4917.

(7) Bar, G.; Magonov, S. N.; Cantow, H.-J.; Kushch, N. D.; Yagubskii, E. B.; Liang, W.; Ren, J.; Whangbo, M.-H. *New J. Chem.*, in press.

(8) (a) Wacker, K.; Buck, P. *Mater. Res. Bull.* 1980, 15, 1105. (b) Wacker, K.; Salk, M.; Decker-Schultheiss, G.; Keller, E. *Z. Anorg. Allg. Chem.* 1991, 606, 51.

(9) Stocker, W.; Salk, M.; Wacker, K.; Magonov, S. N.; Cantow, H.-J. *Adv. Mater.* 1992, 4, 359.

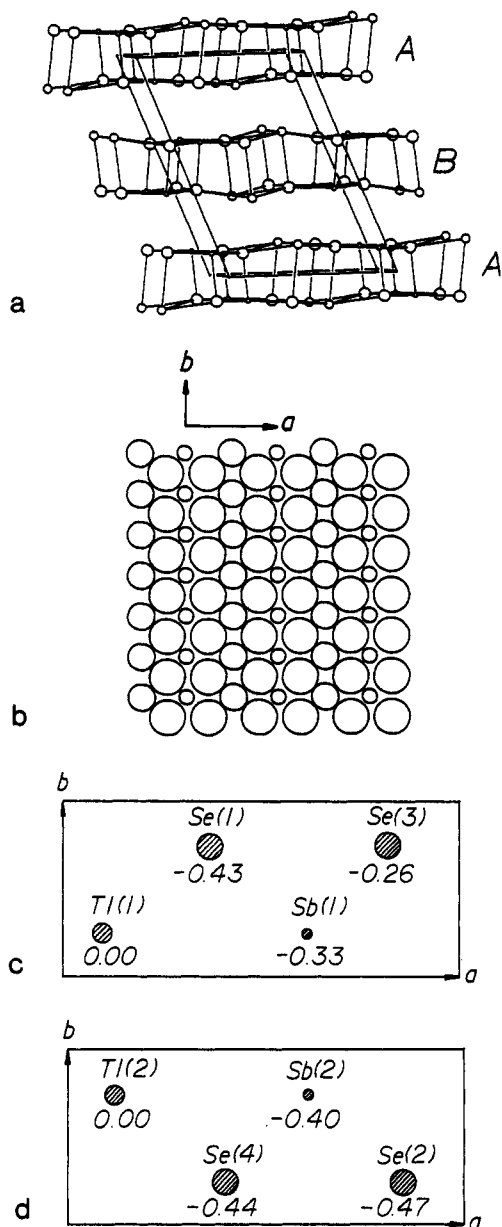


**Figure 1.** (a) Schematic view (along the direction close to the  $b$  axis) of the crystal structure of  $\text{TlSbSe}_2$ , which has two slightly different layers A and B per unit cell. (b) Projection view (in the  $ab$  plane) of the surface sheet atoms of  $\text{TlSbSe}_2$ , where the large, medium and small circles represent the Se, Tl and Sb atoms, respectively. (c) Relative heights in angstroms of the Tl, Sb, and Se atoms on the surface sheet of  $\text{TlSbSe}_2$  layer A. (d) Relative heights in angstroms of the Tl, Sb, and Se atoms on the surface sheet of  $\text{TlSbSe}_2$  layer B.

(responsible for the STM images) changes from Tl to Se within the energy range of 0.17 eV. This implication has not yet been verified by electronic structure calculations. In addition, we note that it is not easy to interpret the STM images of  $\text{TlSbSe}_2$  on the basis of its crystal structure alone. The ionic radii of the  $\text{Tl}^+$  and  $\text{Sb}^{3+}$  ions are much smaller than that of the  $\text{Se}^{2-}$  anion (e.g., 1.98, 1.50, and 0.76 Å for the  $\text{Se}^{2-}$ ,  $\text{Tl}^+$ , and  $\text{Sb}^{3+}$  ions in six-coordinate environments, respectively,<sup>10</sup> so that the effective heights of the  $\text{Tl}^+$  and  $\text{Se}^{2-}$  ions on the surface atom sheet of  $\text{TlSbSe}_2$  may be considered similar. The diffuseness of the valence atomic orbitals decreases in the order  $\text{Tl} > \text{Sb} > \text{Se}$  because their principal quantum numbers decrease in the same order. Then, the effective heights on the

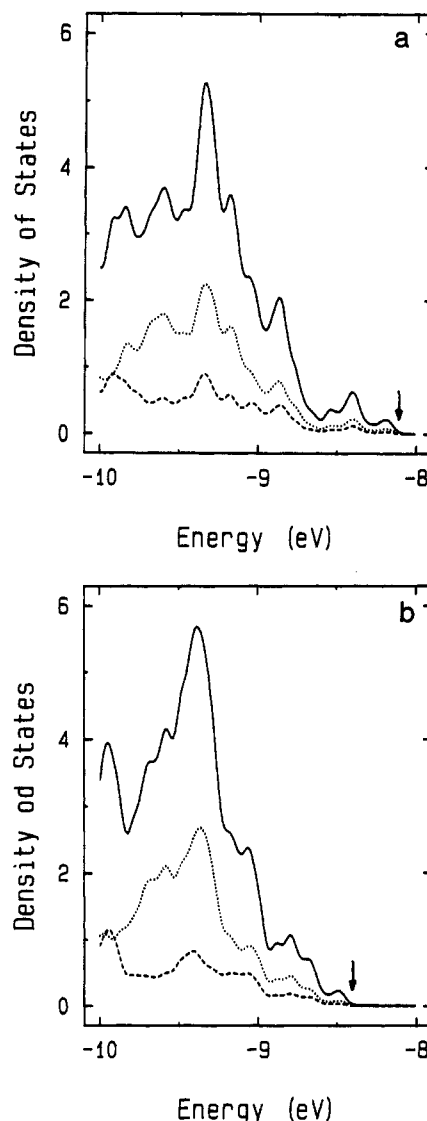


**Figure 2.** (a) DOS plot calculated for a single  $\text{TlSbSe}_2$  layer A. (b) DOS plot calculated for a single  $\text{TlSbSe}_2$  layer B. Only the top portion of the occupied bands is shown, and the arrow indicates the top of the occupied bands. The solid line represents the total DOS, while the dotted and dashed lines refer to the partial DOS values of the Tl and Sb atoms, respectively.

surface atom sheets of  $\text{TlSbSe}_2$  may decrease in the order  $\text{Tl} > \text{Sb} > \text{Se}$ .

In the present work, we study how the STM and AFM images of  $\text{TlSbSe}_2$  can be rationally interpreted. To achieve this objective, the STM and AFM images of  $\text{TlSbSe}_2$  were measured and analyzed on the basis of the  $\rho(r_0, e_f)$  and  $\rho(r_0)$  plots of the individual layers A and B. These density plots were obtained by performing extended Hückel tight binding band (EHTB) electronic band structure calculations.<sup>11</sup>

### Experimental Section

A modified Bridgman–Stockborger technique was used for the crystal growth of  $\text{TlSbSe}_2$ .<sup>8</sup> An appropriate choice of synthesis conditions leads to n-type semiconducting crystals (i.e., the room-temperature ordered phase) with a shape of platelets. These samples exhibit a higher conductivity than do p-type semiconducting crystals and hence are more suitable for STM measurements.

(10) Shannon, R. D. *Acta Crystallogr.* 1976, A32, 751.

(11) Whangbo, M.-H.; Hoffmann, R. *J. Am. Chem. Soc.* 1978, 100, 6093.

**Table I. Exponents  $\zeta_i$  and the Valence Shell Ionization Potentials  $H_{ii}$  for Slater Type Atomic Orbitals  $\chi_i^a$** 

$\chi_i$	$\zeta_i$	$H_{ii}$ (eV)
Tl 6s	2.30	-12.7
Tl 6p	1.60	- 5.8
Sb 5s	2.32	-18.8
Sb 5p	2.00	-11.7
Se 4s	2.44	-20.5
Se 4p	2.07	-13.2

<sup>a</sup>  $H_{ii}$ 's are the diagonal matrix elements  $\langle \chi_i | H^{\text{eff}} | \chi_i \rangle$ , where  $H^{\text{eff}}$  is the effective Hamiltonian. In our calculations of the off-diagonal matrix elements  $H_{ij} = \langle \chi_i | H^{\text{eff}} | \chi_j \rangle$ , the weighted formula was used. For details, see: Ammeter, J. H.; Bürgi, H.-B.; Thibeault, J.; Hoffmann, R. *J. Am. Chem. Soc.* 1978, 100, 3686.

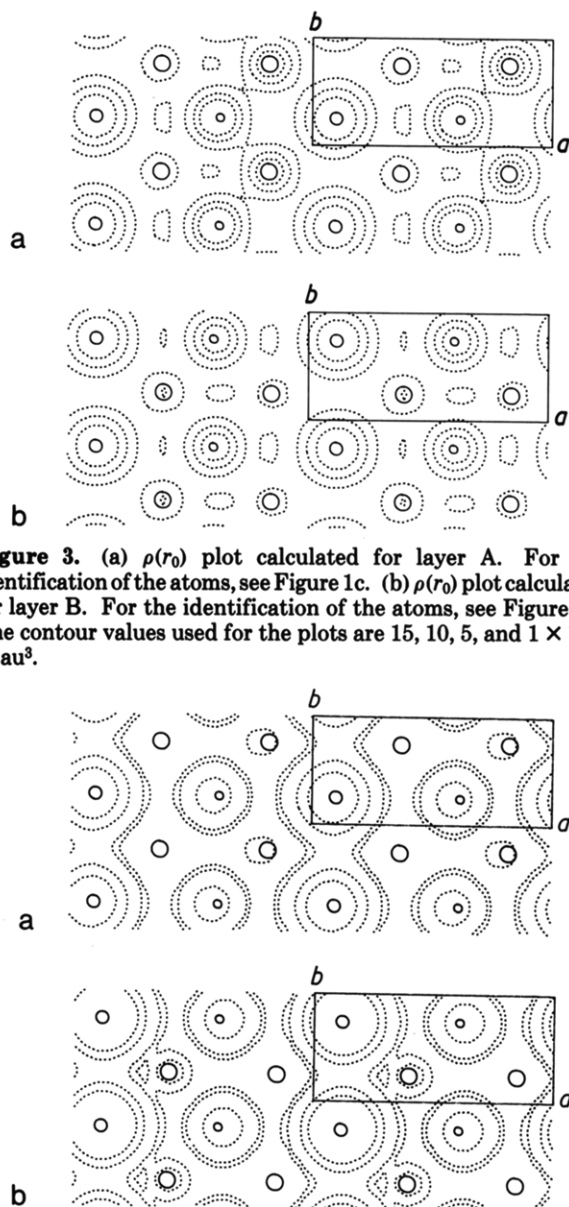


**Figure 3.** (a)  $\rho(r_0)$  plot calculated for layer A. For the identification of the atoms, see Figure 1c. (b)  $\rho(r_0)$  plot calculated for layer B. For the identification of the atoms, see Figure 1d. The contour values used for the plots are 15, 10, 5, and  $1 \times 10^{-3}$  e-/au<sup>3</sup>.

**Figure 4.** (a)  $\rho(r_0, e_t)$  plot calculated for layer A. For the identification of the atoms, see Figure 1c. (b)  $\rho(r_0, e_t)$  plot calculated for layer B. For the identification of the atoms, see Figure 1d. The contour values used for the plots are 100, 50, 10, and  $5 \times 10^{-5}$  e-/au<sup>3</sup>.

A commercial scanning probe microscope, Nanoscope II, was used in our experiments at ambient conditions. Crystals of TlSbSe<sub>2</sub> were fixed to a copper support with conducting glue, and STM and AFM measurements were carried out on a new surface prepared by cleaving. The measured crystal surface corresponds to the crystallo-

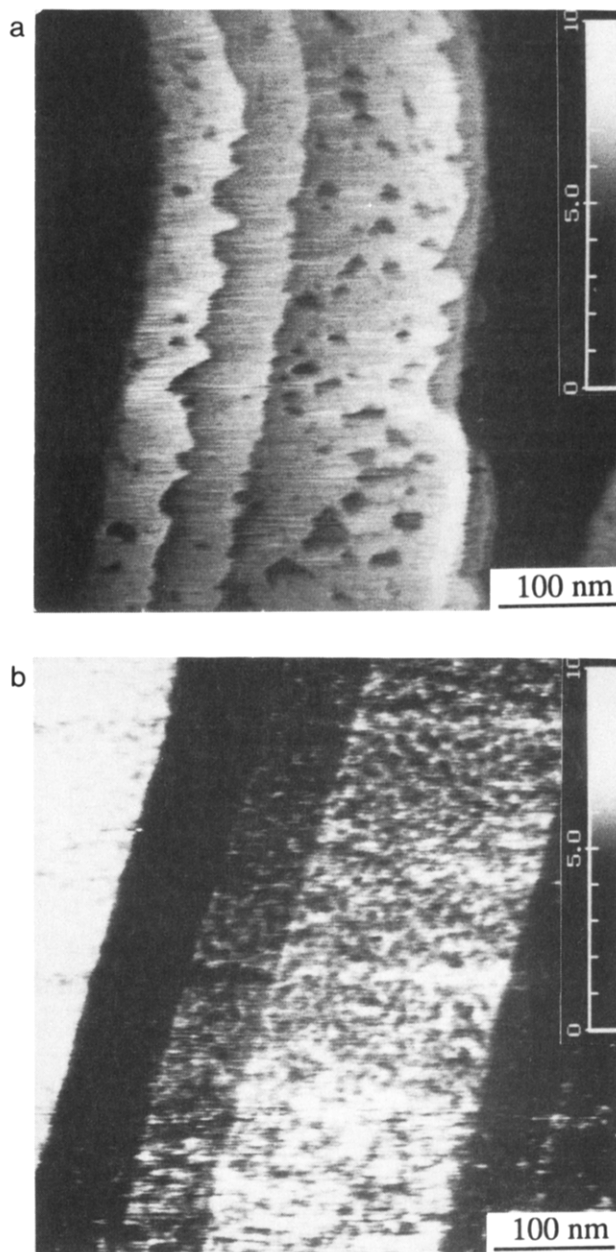


**Figure 5.** (a) Large-scale STM height image on the surface of TlSbSe<sub>2</sub> crystal at tunneling current  $I_{\text{tun}} = 1.0$  and bias voltage  $V_{\text{bias}} = -0.9$  V. The vertical gray-scale bar indicates the height corrugations in nm. (b) Large-scale AFM height image on the surface of TlSbSe<sub>2</sub>. The vertical gray-scale bar indicates the height corrugations in nm.

graphic *ab* plane. Mechanically-sharpened Pt/Ir tips were used for STM, and commercial Si<sub>3</sub>N<sub>4</sub> probes for AFM. STM measurements for n-type TlSbSe<sub>2</sub> crystals were possible only at negative bias voltages (i.e., for the surface-to-tip tunneling), and stable images were observed at bias voltages lower than -0.8 V.<sup>9</sup> The surface morphology of TlSbSe<sub>2</sub> registered in large scale STM and AFM images (up to 1  $\mu\text{m}^2$ ) is characterized by multiple steps (see below). Atomic-scale images were collected on flat terraces.

STM images were obtained in the height and current imaging modes, and AFM images in the height and force imaging modes. The choice of the imaging modes is determined by adjusting the gain parameters of the negative feedback, which controls the vertical motion of the probe. In the AFM measurements the sample was rotated with respect to scanning direction to improve the quality of the image. The atomic-scale images were filtered

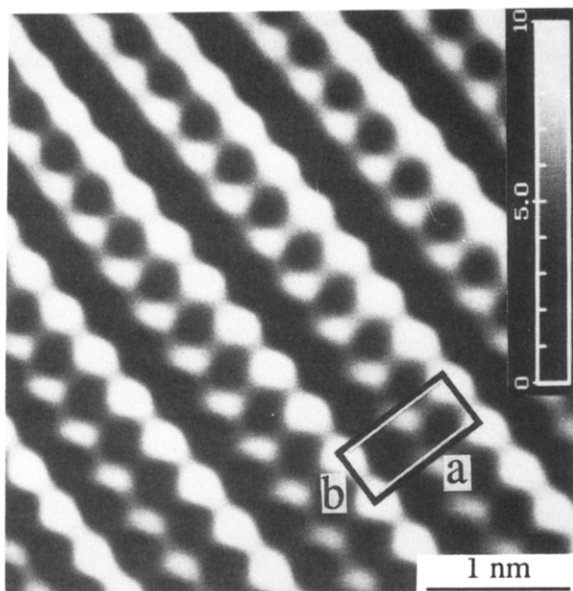
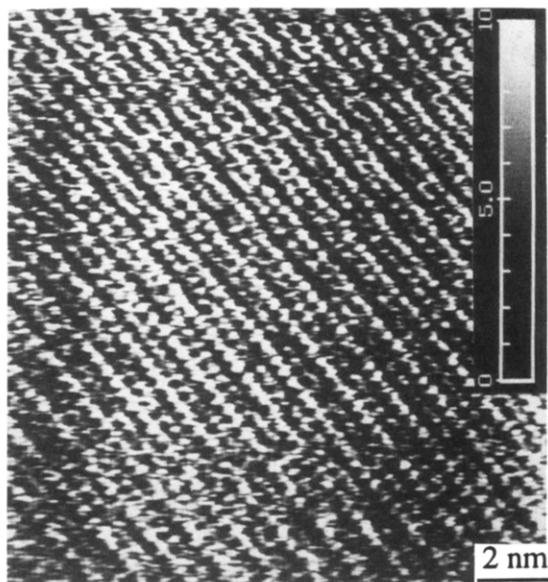


**Figure 6.** (a) AFM height image of  $\text{TlSbSe}_2$ . The vertical gray-scale bar indicates the height corrugations in nm. (b) Zoomed part of the image after FFT filtering.

with the fast Fourier transform (FFT) procedure to emphasize the details of the periodic patterns. The STM and AFM images measured for a same sample may not refer to an identical layer, because the measurements are not necessarily carried out on an identical terrace of the surface.

In STM measurements of a poorly conducting sample such as  $\text{TlSbSe}_2$ , a significant voltage drop can occur when the tip is not close to an electrical contact to the sample surface. This effect can change the tunneling conditions optimal for obtaining well-resolved atomic-scale STM images. In the present work, we attempted to reduce this effect by making a silver glue contact on a freshly cleaved surface of the sample and positioning the tip close to this contact. Under this experimental condition, well-resolved STM images were obtained only at bias voltages between  $-0.9$  and  $-1.2$  V (with set tunneling currents,  $I_{\text{tun}}$ , of  $\sim 1$  nA). These optimal bias voltages, which were verified for more than 10 crystal samples, are somewhat higher than those reported earlier by Stocker et al. (i.e., between  $-1.65$  and  $-1.82$  V).<sup>9</sup>

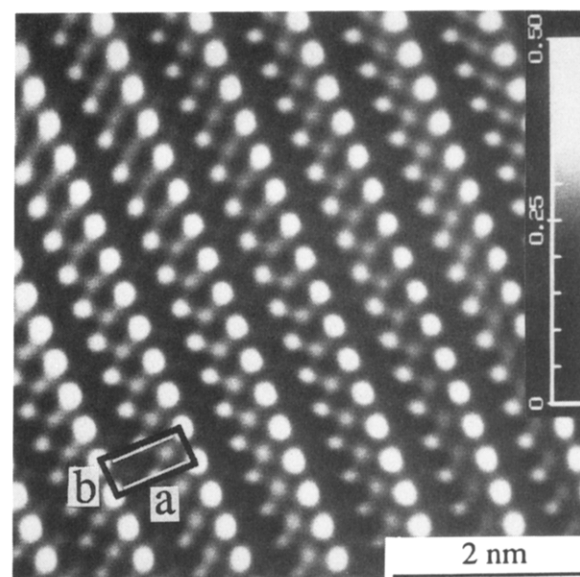
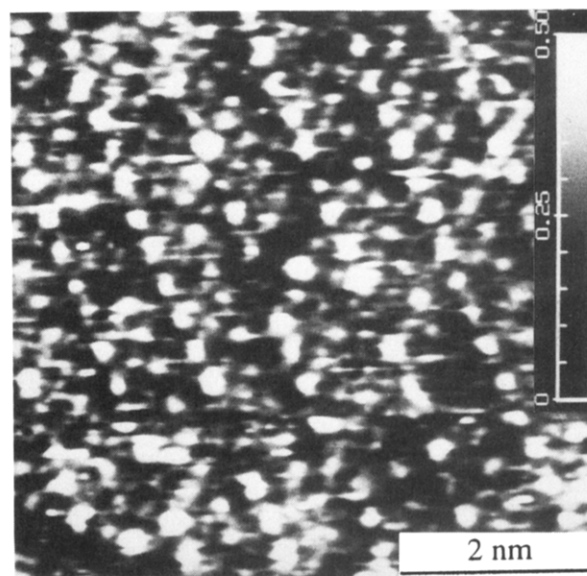


**Figure 7.** (a) STM current image of  $\text{TlSbSe}_2$  at  $I_{\text{tun}} = 1.1$  nA and  $V_{\text{bias}} = -1.2$  V. The vertical gray-scale bar indicates the variation of the image current. The latter is proportional to  $\ln(I)$ , where  $I$  is the actual tunneling current. (b) Image of (a) after FFT filtering.

### Calculations

Our EHTB calculations with the atomic parameters summarized in Table I predict that  $\text{TlSbSe}_2$  is a semiconductor with an indirect bandgap of  $0.58$  eV, which is in reasonable agreement with the experimental bandgap  $0.82$  eV.<sup>12</sup> The plots of the density of states (DOS) calculated (for the top portion of the occupied bands) for the individual layers A and B are presented in parts a and b of Figure 2, respectively. The electronic structures of the two layers are quite similar, and there occurs no abrupt change in orbital composition in the energy range between  $0.5$  and  $1.0$  eV below the valence band top. In our calculations of  $\rho(r_0)$  and  $\rho(r_0, e_f)$ , the tip-to-surface distance  $r_0$  was taken to be  $1.2$  Å from the Tl atom position.

The  $\rho(r_0)$  plots calculated for  $\text{TlSbSe}_2$  layers A and B are shown in parts a and b of Figure 3, respectively. These plots are quite different in that layer B has a high electron density distribution only at the Tl and Sb atoms, but layer A has one not only at the Tl and Sb atoms but also at one of the two Se atoms [i.e., Se(3)]. In layer A the height of Sb(1) is lower than that of Se(3), but the valence atomic

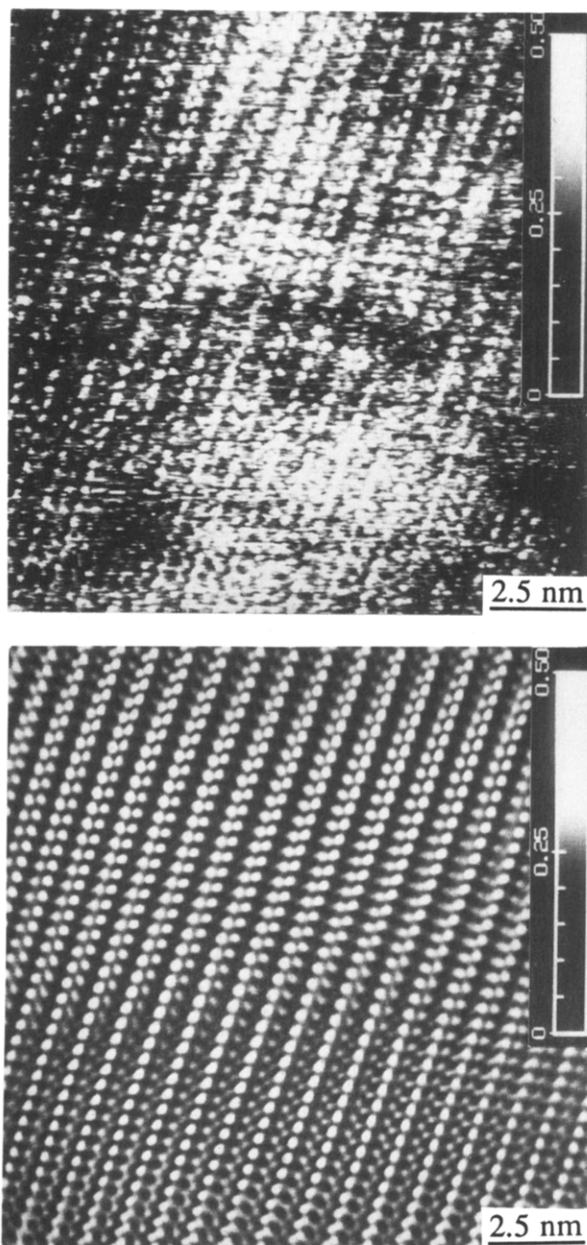


**Figure 8.** (a) STM current image of TlSbSe<sub>2</sub> at  $I_{\text{tun}} = 1.0$  nA and  $V_{\text{bias}} = -0.9$  V. The vertical gray-scale bar indicates the variation of the image current. The latter is proportional to  $\ln(I)$ , where  $I$  is the actual tunneling current. (b) Image of (a) after FFT filtering.

orbitals of Sb are more diffuse than those of Se. Consequently, the Sb(1) and Se(3) contributions are similar in the  $\rho(r_0)$  plot of layer A.

The electron tunneling of TlSbSe<sub>2</sub> is observed only in the surface-to-tip direction, so that we calculate the  $\rho(r_0, e_f)$  plots associated with the top portion of the highest occupied bands of the layers A and B. Since TlSbSe<sub>2</sub> is an n-type semiconductor, its Fermi level should be close to the bottom of the lowest unoccupied band. Consequently, the finding<sup>9</sup> that stable STM images are observed only at bias voltages lower than  $-0.8$  V suggests that the bandgap of TlSbSe<sub>2</sub> is at least 0.8 eV, in agreement with the fact that the band gap of TlSbS<sub>3</sub> is 0.82 eV.<sup>12</sup> The bias voltages used for the present STM measurements are  $-0.9$  and  $-1.2$  eV (see Experimental Section and below),

while those for the work of Stocker et al. are  $-1.65$  and  $-1.82$  eV.<sup>9</sup> Since the bandgap is about 0.82 eV, the  $e_f$  levels appropriate for the calculations of the  $\rho(r_0, e_f)$  plots for  $V_{\text{bias}} = -0.90, -1.20, -1.65,$  and  $-1.82$  eV are the levels lying approximately 0.08, 0.38, 0.83, and 1.00 eV below the valence band top, respectively. In our calculations, the  $\rho(r_0, e_f)$  plots were obtained by sampling the band levels lying within 0.125 eV of these  $e_f$  values. The essential features of the  $\rho(r_0, e_f)$  plots calculated for these plots are similar, so that the atom-selective imaging proposed for TlSbSe<sub>2</sub><sup>9</sup> is not supported. In the following, we present only the  $\rho(r_0, e_f)$  plots calculated for the  $e_f$  level lying 0.38 eV below the valence band top.

The  $\rho(r_0, e_f)$  plots calculated for the layers A and B are shown in parts a and b of Figure 4, respectively. For both layers, these plots are similar: A high electron density is found on the Tl and Sb atoms. The Tl atoms have a larger density than do the Sb atoms. Of the two Se atoms per unit cell, only one is found to have some density in both layers A and B [the Se(3) atoms in layer A and the Se(4) atoms in layer B].

### STM and AFM Images

Large-scale STM and AFM images of TlSbSe<sub>2</sub> are shown in parts a and b of Figure 5, respectively. Terraces with numerous holes characterize the surface morphology of TlSbSe<sub>2</sub>. Slow surface modification was observed in STM experiments, which leads to an erosion of the top layers especially on the step borders.

An atomic-scale AFM image and its zoomed part after FFT filtering are presented in Figure 6. The rows of patterns aligned along the  $b$ -axis direction exhibit different contrasts. The arrangement of the patterns is consistent with the crystallographic parameters of the  $ab$  plane (the main crystallographic parameters are  $a = 9.137$  Å,  $b = 4.097$  Å,  $c = 12.765$  Å,  $\beta = 111.75^\circ$ ):<sup>8</sup> The average distance between the rows of brighter spots,  $9.2 \pm 0.2$  Å, is close to the crystallographic  $a$  parameter. The repeat distance along the rows,  $3.9 \pm 0.1$  Å, corresponds to the  $b$  parameter. Variations in the contrast of the images were observed during measurements at different rotation angles, but the main features of the images (i.e., two patterns per unit cell) remained the same. The comparison of the AFM image with the  $\rho(r_0)$  plots strongly suggests that the observed surface is layer B, and that the brighter rows are associated with the Tl atoms, and the less bright ones with the Sb atoms.

One of the most resolved STM images is presented in Figure 7. Numerous defects appear as vacancies in the periodic patterns of the images. The STM image after FFT filtering (Figure 7b) shows two rows of bright spots per unit cell. In addition, a row of dim spots occurs between every two such bright rows, and the dim spots are displaced along the  $b$  direction by  $b/2$  with respect to the bright ones. The periodicity along the  $b$  direction is  $4.1 \pm 0.4$  Å, and the separation between the brightest rows is  $9.8 \pm 0.2$  Å. This feature is consistent with the crystallographic parameters of TlSbSe<sub>2</sub>. On the basis of the  $\rho(r_0, e_f)$  plots, the bright spots are assigned to the Tl and Sb atoms, with the brighter ones to the Tl atoms. The dim spots are then assigned to one of the two rows of the Se atoms. Consequently, the surface observed by STM is consistent with both layers A and B.

The STM image of Figure 8a (obtained with a sample different from the one used to record the image of Figure 7) reveals numerous imperfections such as vacancies and

(12) (a) Banys, J.; Grigas, J.; Valiukenas, V.; Wacker, K. *Solid State Commun.* 1992, 82, 633. (b) Gitsu, D. V.; Grincheshen, I. N.; Krasovskiy, V. F.; Popovich, N. S. *Sov. Phys. Fiz. Polupr.* 1988, 22, 152.

contrast variations. Figure 8b emphasizes the periodic features of this image after FFT filtering. The STM pattern in the lower part is similar to that expected on the basis the crystallographically perfect layer A (Figures 4 and 7). However, the upper part of the image is difficult to explain, because the pattern appears as if the rows of the Sb atoms became as bright as those of the Tl atoms. It is possible that double tip effects play a role in the images of Figure 8. The occurrence of double tip effects is typically indicated by double patterns in an FFT power spectrum. However, we have not observed such patterns from the FFT power spectrum of Figure 8 (not shown). Further studies are needed to understand what causes such an image variation.

#### Concluding Remarks

The surface of  $\text{TlSbSe}_2$  is complex in terms of both atomic composition and surface corrugation. Nevertheless,

it was possible to explain several essential features of the atomic-scale AFM and STM images with the help of the  $\rho(r_0, e_f)$  and  $\rho(r_0)$  plots calculated for individual  $\text{TlSbSe}_2$  layers. It is clear that, for a surface consisting of several chemically different atoms, the surface topography as determined by AFM can be quite different from that predicted on the basis of the crystal structure. In both STM and AFM images, the brightest spots arise from the most protruded surface atoms, the Tl atoms. The electronic structure of  $\text{TlSbSe}_2$  does not support the proposal<sup>9</sup> that there occurs an atom-selective imaging in the STM images when the bias voltage changes from  $-1.65$  to  $-1.82$  eV.

**Acknowledgment.** We thank Dr. K. Wacker and M. Salk for  $\text{TlSbSe}_2$  samples. The work at North Carolina State University was supported by the Office of Basic Energy Sciences, Division of Materials Sciences, U.S. Department of Energy, under Grant DE-FG05-86ER45259.